



2nd Advanced Optical Metrology Compendium

Advanced Optical Metrology

Geoscience | Corrosion | Particles | Additive Manufacturing: Metallurgy, Cut Analysis & Porosity



EVIDENT
OLYMPUS

WILEY

The latest eBook from **Advanced Optical Metrology**.
Download for free.

This compendium includes a collection of optical metrology papers, a repository of teaching materials, and instructions on how to publish scientific achievements.

With the aim of improving communication between fundamental research and industrial applications in the field of optical metrology we have collected and organized existing information and made it more accessible and useful for researchers and practitioners.

EVIDENT
OLYMPUS

WILEY

Designing Artificial Fluorescent Proteins: Squaraine-LmrR Biophosphors for High Performance Deep-Red Biohybrid Light-Emitting Diodes

Sara Ferrara, Sara H. Mejias, Mantas Liutkus, Giacomo Renno, Francesca Stella, Irene Kociolek, Juan Pablo Fuenzalida-Werner, Claudia Barolo,* Pedro B. Coto,* Aitziber L. Cortajarena,* and Rubén D. Costa*


Biophosphors with fluorescent proteins (FPs) are promising candidates to replace rare-earth color down-converting filters for white light-emitting diodes (LEDs). There is, however, a lack of deep-red FPs meeting high photostabilities, photoluminescence quantum yields (ϕ), and throughput expression yields. Herein, a new approach for the design of highly emissive and stable deep-red biophosphors combining an artificial FP (Lactococcal multidrug resistance Regulator (LmrR) as protein host and an archetypal red-emitting squaraine (S) as guest) with a polymer network is demonstrated toward high performing deep-red biohybrid LEDs (Bio-HLEDs). At first, the best protein pocket (aromaticity, polarity, charge, etc.) to stabilize S in water is determined using four LmrR variants (position 96 with tryptophan, histidine, phenylalanine, and alanine). Computational and time-resolved spectroscopic findings suggest that the tryptophan is instrumental toward achieving artificial red-emitting FPs with $\phi > 50\%$ stable over weeks. These features are further enhanced in the polymer coating ($\phi > 65\%$ stable over months) without affecting emission color. Finally, deep-red Bio-HLEDs are fabricated featuring external quantum efficiencies of 7% and stabilities of ≈ 800 h. This represents threefold enhancement compared to reference devices with S-polymer color filters. Overall, this work highlights a new design for highly emissive deep-red biophosphors, achieving record performance in deep-red protein-LEDs.

1. Introduction

Inorganic and organic light-emitting diodes (ILEDs and OLEDs, respectively) are quickly replacing incandescent light bulbs and compact fluorescent lamps.^[1–3] On one hand, ILEDs' performance has met the market requirements for in-/out-door applications with single-point sources. However, there are severe concerns with respect to their sustainability due to i) the employment of either rare-earth or toxic color down-converting filters or inorganic phosphors (IPs), ii) the high-cost and environmental unfriendly fabrication conditions of both the phosphor and the emitting chip, and iii) the lack of efficient recycling protocols.^[4–6] On the other hand, the OLED technology is very promising for large-area and flexible lighting applications. Nevertheless, the need of i) a multilayered structure prepared partially via evaporation techniques, ii) stable blue-emitters, and iii) enhanced light-outcoupling and protective encapsulation barriers, make OLEDs very expensive for widespread use.^[7,8]

S. Ferrara, J. P. Fuenzalida-Werner, R. D. Costa
Chair of Biogenic Functional Materials
Technical University of Munich
Schulgasse 22, 94315 Straubing, Germany
E-mail: ruben.costa@tum.de

S. H. Mejias, M. Liutkus, A. L. Cortajarena
Center for Cooperative Research in Biomaterials (CIC biomaGUNE)
Basque Research and Technology Alliance
Donostia-San Sebastián 20014, Spain
E-mail: alcortajarena@cicbiomagune.es

 The ORCID identification number(s) for the author(s) of this article can be found under <https://doi.org/10.1002/adfm.202111381>.

© 2022 The Authors. Advanced Functional Materials published by Wiley-VCH GmbH. This is an open access article under the terms of the Creative Commons Attribution-NonCommercial License, which permits use, distribution and reproduction in any medium, provided the original work is properly cited and is not used for commercial purposes.

DOI: 10.1002/adfm.202111381

G. Renno, F. Stella, I. Kociolek, C. Barolo
Department of Chemistry
Università degli Studi di Torino
Via Giuria 7, Torino 10125, Italy
E-mail: claudia.barolo@unito.it

G. Renno, F. Stella, I. Kociolek, C. Barolo
NIS Interdepartmental Centre and INSTM Reference Centre
Università degli Studi di Torino
Via Gioacchino Quarello 15/a, Torino 10125, Italy

C. Barolo
ICxT Interdepartmental Centre
Università degli Studi di Torino
Lungo Dora Siena 100, Torino 10153, Italy

P. B. Coto
Materials Physics Center (CFM)-Spanish National Research Council (CSIC) and Donostia International Physics Center (DIPC)
Paseo Manuel de Lardizabal 5, Donostia-San Sebastián 20018, Spain
E-mail: pedro.brana@csic.es

In this scenario, hybrid LEDs (HLEDs) have been reborn, promising to achieve sustainable lighting systems without losses in device performance.^[9–14] They aim at replacing IPs with organic color down-converting filters or organic phosphors (OPs) that combine organic emitters (e.g., small molecules, coordination complexes, polymers, or carbon dots, among others) with polymers, metallic organic frameworks (MOFs), etc., as packaging matrices.^[15–23] Though this field started at the beginning of the 21st century, several recent advances have set in their relevance. Among them, new efficient and stable OPs, such as iridium(III) complexes-silica nanoparticles,^[24] benzodimidazole-based systems for green HLEDs,^[25] stable perovskite-based filters,^[26,27] and biophosphors implementing biogenic components^[28,29] stand out compared to the prior art. Indeed, BASF has launched a new series of HLED lamp systems based on the Sunvue technology.

Concerning biophosphors, three families have been developed to date. In a chronological order, artificial emitters were firstly dispersed in biogenic matrices, such as deoxyribonucleic acid,^[30] proteins,^[31] polysaccharides,^[32] and cellulose,^[33] reaching maximum efficiencies of ≈ 35 lm W⁻¹. Secondly, the Bio-HLED concept was settled when fluorescent proteins (FPs) were stabilized in polymer coatings, resulting in <10% intensity loss after 100 h of operation.^[28,34,35] Enhancing the polymer matrix has led to Bio-HLEDs with stabilities >150 days at ≈ 130 lm W⁻¹.^[29] Several groups have further developed Bio-HLEDs employing different natural^[36,37] and artificial FPs (AFPs).^[31,38,39] Finally, fully biogenic phosphors, in which both the packaging matrix and the emitter are of biological origin (e.g., silk fibroin (SF) as packaging matrix and FPs as emitters) have been recently reported,^[40] achieving efficiencies of 40 lm W⁻¹ and stabilities of 1.2 and 500 h (200 mA) for on chip and remote configurations, respectively.

A major bottleneck in Bio-HLEDs is to find highly efficient and stable red-emitting FPs.^[41] Among them, mCherry has been widely used as a representative candidate, as it combines good photophysical features ($\phi = 22\%$), high expression yields, and excellent pH tolerance;^[9,14,42,43] though this still falls short for lighting applications. Thus, new strategies to design highly emissive and stable deep-red AFPs are needed. It is here where the major thrust of this work sets in with a new red-emitting AFP combining a Lactococcal multidrug resistance Regulator (LmrR) as a protein host with a symmetric and non-water soluble archetypal squaraine dye (S) as a guest emitter (**Figure 1**). LmrR is a homodimeric protein with a β -winged helix-turn-helix structure (**Figure 1a**). The two chains form a large hydrophobic pocket suitable for supramolecular assemblies promoted by hydrophobic interactions with the pocket and/or π - π interactions with the indole rings of the two tryptophan residues, without requiring covalent co-factor attachment. Indeed, LmrR has shown high versatility

to accommodate organic dyes with different structures.^[44] Both, the lack of needing covalent co-factor attachment and the nonspecific nature of complexation, allow for easy dye screening, making LmrR a potential scaffold to generate a highly stable AFP. Up, squaraines as host emitters in proteins have already been widely adopted as biological probes, but the preparation of LmrR-S assemblies has not been realized yet.^[45] The resonance-stabilized zwitterionic structure of S (**Figure 1a**) with a strong emission in the far-red region makes this dye very attractive for deep-red AFPs.

In this context, this work describes the optimized design of AFPs based on LmrR-S and their respective biophosphors realizing Bio-HLEDs outperforming both the prior-art in red-Bio-HLEDs and the reference devices with just S-based OPs. The LmrR-S affinity was optimized by substituting the tryptophan at position 96 (W96) of the protein cavity with histidine (W96H), phenylalanine (W96F), or alanine (W96A), leading to the AFPs W96-S, W96H-S, W96F-S, and W96A-S (**Figure 1a,b**). Joint computational hybrid quantum mechanics/molecular mechanics/molecular dynamics (QM/MM/MD) methods and time-resolved spectroscopic studies allowed to rationalize why the wild-type variant was the only one successful in stabilizing S in both aqueous solution and polymer coatings, leading to photoluminescence quantum yields (ϕ) of $\approx 65\%$ associated to i) an emission centered at 710 nm with x/y Commission internationale de l'éclairage (CIE) color coordinates of 0.66/0.23 (i.e., deep-red region) and ii) stabilities over months. This resulted in highly efficient and stable deep-red Bio-HLEDs compared to reference devices with only S-polymer OPs, achieving external quantum efficiency (EQE) of 7% along with stabilities of 30/800 h using on chip/remote configurations, respectively. Hence, this work describes i) an easy-to-do concept toward stable and efficient red-emitting AFPs following a hybrid host-guest combination of artificial and biogenic moieties, ii) a new route toward highly performing water processable red biophosphors using emitters that are otherwise soluble in toxic solvents, and iii) the best performing deep-red Bio-HLED reported to date.

2. Results and Discussion

2.1. Synthesis and Characterization of Red-Emitting LmrR-S Proteins

S was synthesized under microwave irradiation through the condensation reaction between the squaric acid and an indolenine quaternary compound following published protocols (yield after two steps 43%).^[46] Four different LmrR mutants were constructed to probe the protein pocket affinity to S and how the host-guest interactions affect the photophysical properties in aqueous solutions. W96A was used to assess a purely hydrophobic pocket, W96H mutant probed the effects of a hydrogen donor, while W96 and W96F variants allowed to study the effects of proton donor or non-donor aromatic groups, respectively (**Figure 1**).

LmrR-S AFPs were formed by incubating the water-dispersed S with the protein variants (see the Experimental Section). The structural stability of the protein scaffold in the LmrR-S series was verified by UV circular dichroism, confirming that the structure of LmrR is not affected by either mutation or inclusion

A. L. Cortajarena
Ikerbasque
Basque Foundation for Science
Bilbao 48009, Spain
A. L. Cortajarena
Technische Universität München
Biogenic Functional Materials
Schulgasse 22, 94315 Straubing, Germany

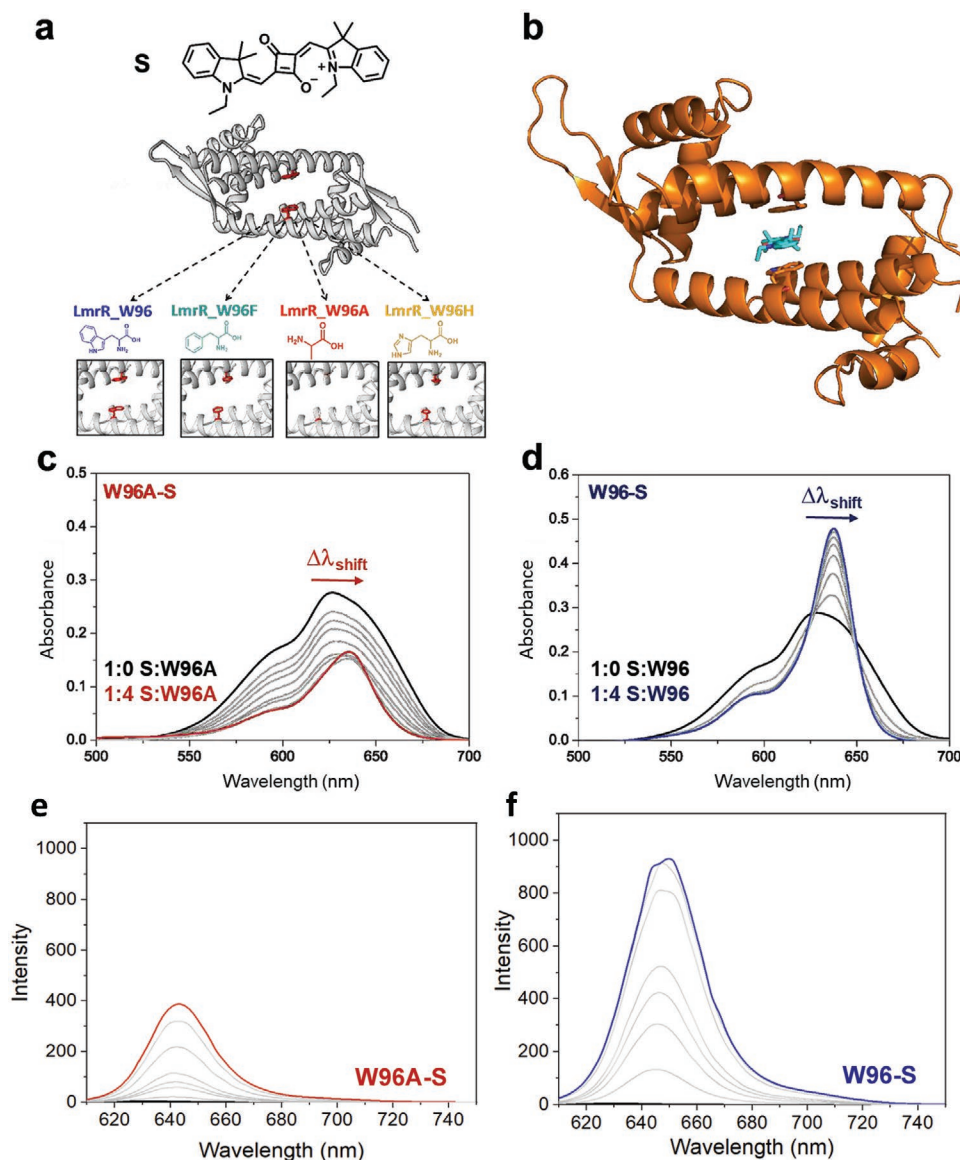


Figure 1. Characterization of LmrR-S assemblies. a) Structures of S dye (top) and the dimeric LmrR (bottom), in which the positions 96 and 96' are highlighted in red for the tryptophan (blue), phenylalanine (green), alanine (red), and histidine (yellow) variants. b) Crystal structure of W96-S with the dye S inside the protein pocket (PDB ID: 7Q34). c–f) Absorption c,d) and emission e,f); excitation wavelength (λ_{exc}) = 590 nm) spectra of S in PBS buffer (12.46×10^{-6} M, black solid line) upon forming the LmrR-S complex when titrated with W96A c,e) and W96 d,f) reaching a molar ratio of 1:4 (see legend).

of S (Figure S1, Supporting Information). The LmrR-S complex showed a slightly better thermal and pH stability than LmrR, revealing the stabilizing effect of S conjugation.

The formation of the LmrR-S was monitored via steady-state absorption and emission spectroscopy (Figure 1; and Figure S2 and Table S1, Supporting Information). In water (phosphate buffer, pH 8), S forms H-type aggregates with the typical broad absorption peak centered at 625 nm and no emission.^[47,48] Upon addition of any LmrR variant (i.e., titration with LmrR:S molar ratio ranging from 0.2 to 4), the interaction of S with LmrR appears in two different spectral changes: i) a decrease in the absorption intensity along with a slight red shift of the maximum of absorption and an increase in the emission intensity caused by electrostatic interactions of the negatively charged part of S with the positively charged surface of LmrR, and ii) a sharpening of

the absorption band in concert with an increase in absorption/emission intensities indicating the incorporation of the S into the hydrophobic protein host cavity. By monitoring absorption intensity (ΔA_{bleach}) and spectral shift ($\Delta \lambda_{\text{shift}}$) changes, the apparent dissociation constant of the electrostatic interaction (K_{de}) and the hydrophobic interaction (K_{dh}) were calculated (see the Experimental Section; and Table S1, Supporting Information).

Wild-type W96 showed the highest binding affinity to host S via hydrophobic interactions with a K_{dh} of 0.02×10^{-6} M. No spectral bleaching was observed with this mutant, indicating very low electrostatic interactions (Figure 1). By contrast, W96A variant featured the highest K_{de} of 0.52×10^{-6} M and K_{dh} of 1.47×10^{-6} M (Figure 1; and Table S1, Supporting Information), suggesting that the stabilization of S must be driven by electrostatic interactions at the protein surface. W96F and W96H

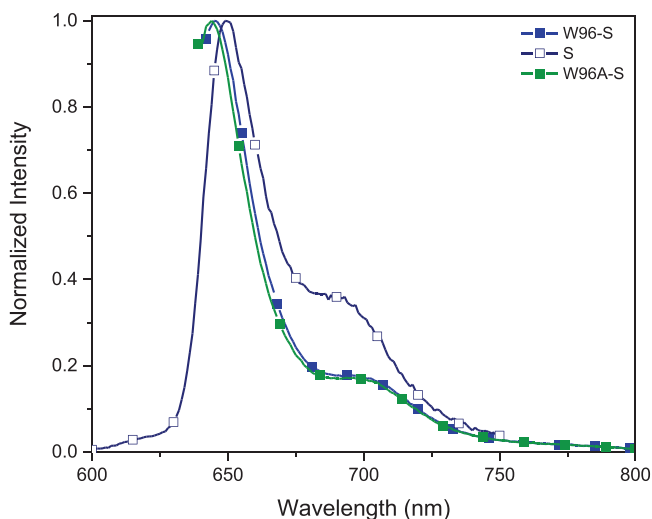


Figure 2. Photoluminescence spectra of W96-S (blue) and W96A-S (green) in aqueous solution ($\lambda_{exc} = 638$ nm; 10^{-5} M) and S (open squares) in acetonitrile solution ($\lambda_{exc} = 590$ nm; 10^{-5} M).

mutants had intermediate K_{de} and K_{dh} values, indicating both modes of interaction contribute to stabilize the LmrR-S complex (Table S1, Supporting Information).

The LmrR-S stability was studied monitoring the absorption spectrum over time and fitting the absorbance difference using an exponential decay function to obtain the bleaching rate constant (K_b ; Figure S3, Supporting Information). The K_b value of 0.015 h $^{-1}$ for W96A-S was comparable to that of free S (0.024 h $^{-1}$), while W96-S exhibited only a small reduction in the intensity that could not be fit by any exponential decay function. Thus, S could be considered efficiently stabilized into the protein cavity in aqueous solution. Final corroboration came from studying the photoluminescence features of W96-S compared to S in acetonitrile. While S featured only a weak (i.e., $\phi < 5\%$) emission due to a prominent vibrational nonradiative deactivation rate (Figure 2),^[49] W96-S showed emission bands centered at 645 and 705 nm associated to $\phi \approx 50\%$ and an excited state lifetime (τ) of ≈ 3.8 ns (Figure 2 and Table 1). Remarkably, W96-S was found to be stable under ambient conditions for a week, suggesting that S is efficiently locked inside and/or shielded by the protein cavity. In addition, W96A-S also exhibited a similar emission spectrum with $\phi < 5\%$ and low stability in aqueous solution, confirming that the stabilization of S via electrostatic interactions at the protein surface is not effective to maintain its emission features. As observed in the molecular dynamics simulations (vide infra), when S goes outside the

protein binding pocket, it gets attached to the surface via weak interactions. As a result, S can undergo large conformational changes leading to nonplanar structures that exhibit poor emission properties. In addition, this conformational flexibility can promote molecular distortions triggering nonradiative deactivation processes.^[50,51] By contrast, S adopts a quasiplanar conformation inside the hydrophobic pocket of the W96 protein, leading to S conformations with good emission properties. This has been confirmed by X-ray crystallography and theoretical studies.

Since the wild-type W96 variant is the strongest S binder, the W96-S complex was selected for further structural and functional studies (see the Experimental Section). The W96-S complex crystallized in an orthorhombic lattice with $P2_12_12_1$ symmetry (Figure 1; and Figure S4 and Table S2, Supporting Information). The asymmetric unit was formed by two protein dimers. All four chains exhibited the characteristic LmrR fold with only minor differences in the flexible loop region, making the chains non-identical (Figure S4, Supporting Information). Best crystals diffracted to only 2.6 Å, worse than some previously reported crystals of LmrR that surpassed 2 Å resolution.^[52–54] This is related to the lattice structure that has large solvent channels and is maintained by very few contacts between protein units, allowing for significant flexibility. In fact, one of the contacts bridging two LmrR dimers is solely maintained by nickel ions binding to His86 residues (confirmed by anomalous scattering). In addition, the protein exhibits flexible loops and the entire C-terminal Strep-tag (≈ 20 amino acids) was not resolved.

In view of the above-mentioned, W96-S retained the characteristic LmrR fold with an open cavity formed by the two protein chains with significant unmodeled electron density in the binding pocket (Figure S5, Supporting Information). Unfortunately, the structural features of the density were not clearly discernible, making it impossible to accurately model S within the LmrR pocket. This issue has been previously reported,^[52,55] as the noncovalent nature of the interaction enables several modes of binding inside the cavity, resulting in an averaged electron density map. However, the overall shape of the electron density suggests that S enters into the binding groove perpendicular to the cavity along the center-line of the pocket without resting along the entire length of the pocket, but only interacting with the symmetrically positioned Trp96 and Asp100 of the two protein chains forming the central region of the pocket. In fact, the tryptophan sidechains adopt a parallel conformation, suggesting the formation of a sandwich-like structure with S (Figure 1). Finally, the binding cavity is not sufficiently deep to accommodate the whole S and, in turn, part of S should be out of the cavity. As the cavity is open on both sides, S can stick

Table 1. Photophysical features of S and W96-S in aqueous solution and polymer coatings (biophosphor).

Compound	Solution					Biophosphor				
	λ_{em} [nm]	ϕ [%]	τ [ns]	$k_r^{a)}$ [s $^{-1}$]	$k_{nr}^{a)}$ [s $^{-1}$]	λ_{em} [nm]	ϕ [%]	τ [ns]	$k_r^{a)}$ [s $^{-1}$]	$k_{nr}^{a)}$ [s $^{-1}$]
S	650–705	<5%	–	–	–	650–705	50	3.9	1.28	1.28
W96-S	645–705	50	3.8	1.32	1.32	665–705	65	5	1.30	0.7

^{a)} $\times 10^8$, emission wavelength - λ_{em} [nm]; photoluminescence quantum yield - ϕ [%], excited state lifetime [ns]; radiative constant - k_r [s $^{-1}$]; non-radiative constant - k_{nr} [s $^{-1}$].

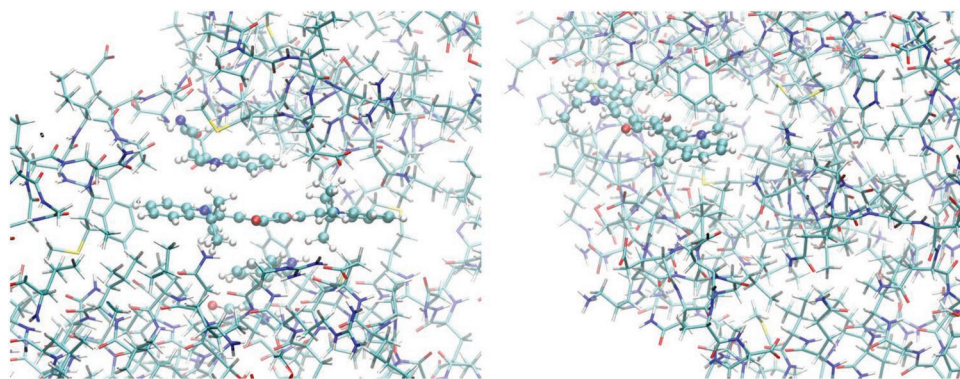


Figure 3. Snapshots taken at the end of the production dynamics run illustrating the locked position of S between the tryptophan residues in the protein cavity of W96-S (left) and on the protein surface after migration outside the protein cavity of W96A-S (right). For clarity, S and the tryptophan residues have been depicted using balls and sticks.

out from either side of the dimer, allowing several different modes of binding. The above-mentioned factors lead to a featureless averaged electron density map and also result in poorer refinement statistics of the final structure (Table S2, Supporting Information).

To further understand S binding inside the protein, QM/MM/MD simulations of the W96-S and W96A-S proteins were carried out (see the Experimental Section). In the simulations, similar structures for W96-S and W96A-S variants were used, in which S was placed inside the protein cavity. The results show that the location of S differs in both systems over the simulation time explored (50 ns). In W96-S a significant part of S is located within the binding pocket partially locked between the tryptophan residues (Figure 3). In addition, the simulations also show that S exhibits large conformational flexibility and some degree of freedom of movement within the binding pocket. This is consistent with the poor X-ray density resolution of S that made it impossible to accurately fit the model. By contrast, S exhibits a larger freedom of movement in the case of W96A-S, displacing to the edges of the protein cavity and toward the protein surface (Figure 3; and Figure S6, Supporting Information). This type of arrangement makes S in W96A-S more exposed to the external aqueous environment than in W96-S. This is in line with the photophysical findings, namely i) the absorption spectral changes between variants (Figure 1) and ii) the low ϕ in W96A-S, as both electrostatic interactions and conformational distortions of S may affect the emission efficiency and promote non-radiative deactivation processes.

2.2. Preparation and Characterization of Deep-Red Bio-HLEDs

The W96-S biophosphors (**1**) were prepared by adding a mixture of linear and branched polyethylene-oxide polymers (mass ratio 4:1) to an aqueous solution of W96-S (1 mg) under strong stirring conditions. This was followed by a gentle vacuum drying process (see the Experimental Section).^[28] For reference purposes, S-polymer phosphors (**2**) were prepared with the same amount of S in acetonitrile following the same procedure. As observed in solution, the emission of **1** corresponds to a well-defined emission shape centered at 665 and 705 nm with $\phi \approx 65\%$ and $\tau \approx 5$ ns (Table 1), remaining constant over months

under ambient conditions (Figure 4). Likewise, **2** featured a similar emission band centered at 650 and 705 nm with $\phi \approx 50\%$ and $\tau \approx 3.9$ ns (Table 1).

At first, deep-red Bio-HLEDs were prepared by combining **1** and **2** with a 590 nm pumping LED chip using an on-chip configuration. Regardless of the applied current in a range from 5 to 200 mA, **1** led to a total conversion of the yellow electroluminescence without an increase in the coating temperature (Figure 5). This resulted in Bio-HLEDs with a deep-red emission featuring a maximum at 705 nm, a full width at half maximum of ≈ 60 nm, and stable x/y CIE color coordinates of 0.66/0.23. The EQE increased up to values of $\approx 7\%$ holding constant from 50 to 200 mA (Figure 5). Likewise, **2** also showed a full conversion of the electroluminescence toward the deep-red region at any applied current, reaching, however, a slightly lower maximum EQE of $\approx 5\%$ from 50 mA due to the lower ϕ (Figure 5; and Figure S7, Supporting Information).

The device stability was investigated using an applied current of 50 mA, corresponding to the maximum EQE for both, **1** and **2**. L_{50} values (i.e., time needed to reach 50% of the initial emission intensity) of around 35 and 20 h were noted for **1**- and **2**-Bio-HLED devices, respectively. In addition, a similar deactivation mechanism is present based on the emission spectra changes over time (Figure 6). In detail, the emission band centered at 705 nm held constant over the first 5 and 15 h

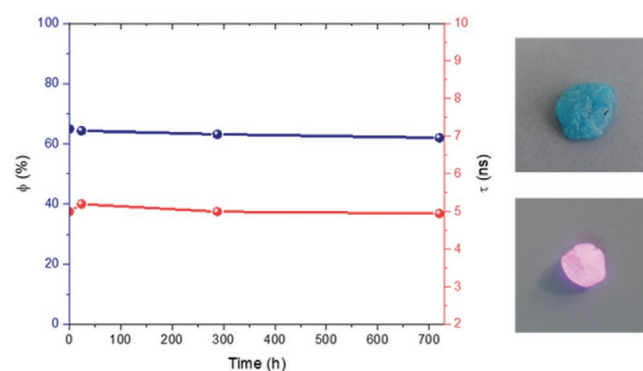


Figure 4. Left: Changes in ϕ (blue) and τ (red) of **1** over time under ambient storage conditions. Right: Picture of **1** under room light (top) and UV-irradiation (bottom).

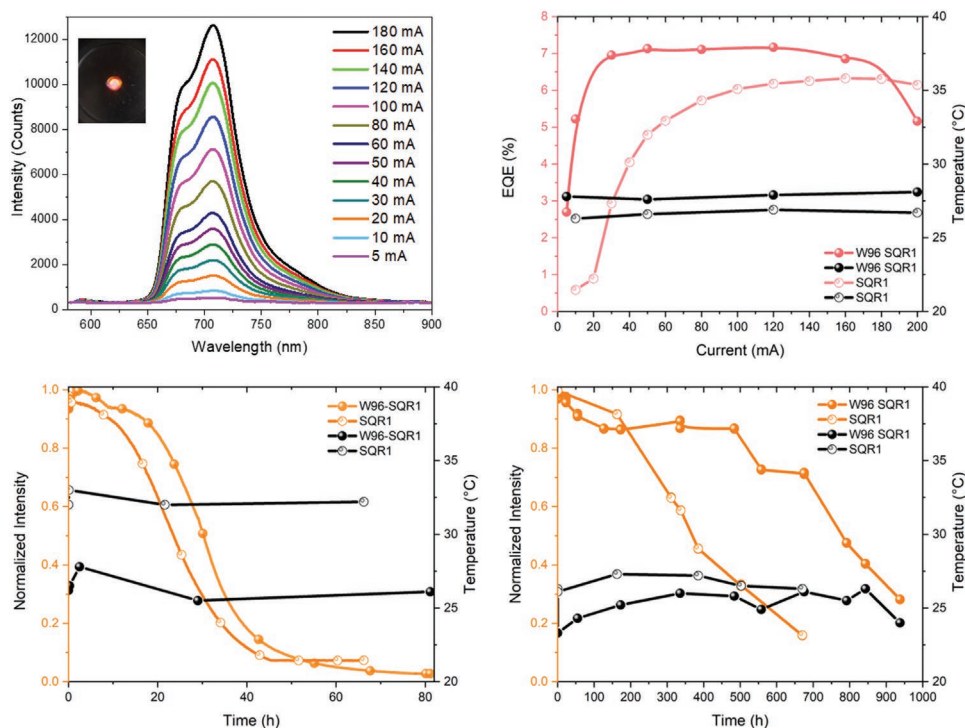


Figure 5. Top: Emission spectra (left) of 1-Bio-HLEDs and EQE/phosphor temperature for 1- and 2-devices (right) at different applied currents. A working device picture is shown in the inset. Bottom: Emission intensity decay/phosphor temperature over time of on chip (left) and remote (right) configurations of 1- and 2-devices at 50 mA under ambient operating conditions.

for 2 and 1-Bio-HLEDs, respectively. Afterward, the vibrational progression of the emission changed toward a dominant vibrational peak centered at 675 nm. At this point, S exhibited the same quick photobleaching with a slight blue shift in the emission band shape. The first process is much faster for reference 2-devices, highlighting the effective shielding effect of the protein cavity. In line with the theoretical simulations, the changes in the vibronic progression might be caused by the rearrangement of S, which is stabilized inside the protein binding pocket mainly by weak (non-covalent) interactions. Under operating conditions, the W96-S system can acquire a sufficient excess of energy to induce the conformational transition of the S moiety from a more locked conformation inside

the protein binding pocket to a more labile structure exposed to the external and more polar matrix environment, ultimately leading to a blueshifted emission and its final photobleaching. Despite these changes, the device chromaticity is only slightly affected over the lifespan of the device (i.e., $\Delta x = 0.06$ and $\Delta y = 0.05$).

To further enhance the device stability, 1-Bio-HLEDs were fabricated using a remote configuration, in which the biophosphor filter was placed at 2 cm from the emitting chip.^[35] Figure 5 depicts an increase of the L_{50} value up to 780 and 320 h for 1 and 2-devices, respectively. Here, the same changes in the emission spectrum noted for the on-chip configuration were present, suggesting that the degradation mechanism is similar.

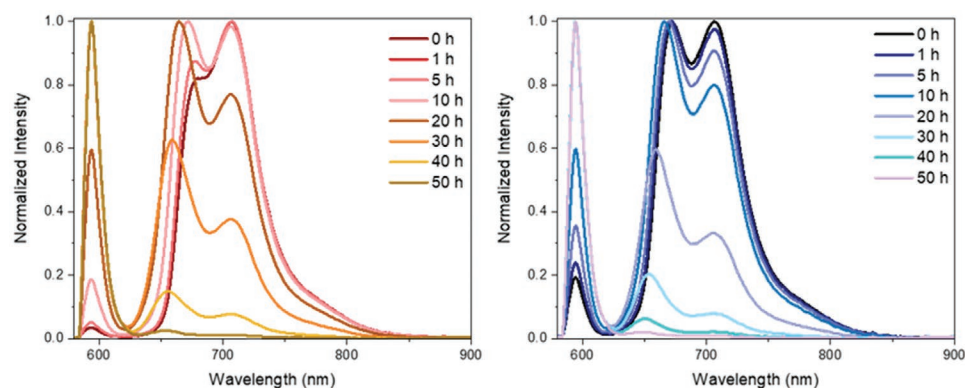


Figure 6. Emission spectra changes over time of 1- (left) and 2- (right) on chip devices at 50 mA and operating under ambient conditions.

In light of the aforementioned, 1-Bio-HLEDs show remarkable performance compared to previously reported red-emitting protein-based LEDs using both FP- and AFP-phosphors.^[9,14]

3. Conclusions

This work sets in the best design of the first deep-red artificial fluorescent protein with LmrR protein (host) and simple squaraine (S) emitter (guest) for biophosphors in protein-based lighting systems. In particular, four mutant variants of LmrR were studied, in which the nature of the cavity of the host protein (aromaticity, polarity, charge, etc.) was explored to finally stabilize the guest S inside the protein cavity via hydrophobic interactions boosted by aromatic rings (i.e., tryptophan), as supported by X-ray structure and QM/MM/MD simulations. This led to enhanced $\phi > 50\%$ stable over weeks; as reference the photoluminescence of S in acetonitrile is characterized by $\phi < 5\%$. This was further enhanced in polymer matrices, realizing biophosphors with a deep-red emission centered at 665 and 705 nm associated to $\phi > 65\%$ stable over months. These excellent features resulted in record deep-red Bio-HLEDs featuring excellent EQE of 7% and stabilities over 800 h.

In view of these results, this work paves the way for the use of ad hoc designed AFPs for lighting applications. While a few examples of devices using natural^[29,35–37] and engineered FPs^[38,56] in both, artificial and biogenic matrices, have recently been reported,^[9,14] this work is a landmark showing that the combination of artificial emitters with selected protein scaffolds represents a promising approach to tackle the limitation of poor emissive FPs toward highly performing deep-red Bio-HLEDs.

4. Experimental Section

Synthesis of S: This dye was prepared following a microwave assisted procedure.^[46]

LmrR Design and Production: The gene for LmrR in pET-17b expression vector was kindly supplied by Prof. Gerard Roelfes (Groningen University, The Netherlands). W96A, W96H, and W96F mutants were created through QuikChange site-directed mutagenesis. Proteins were expressed in *E. coli* C41 (DE3) cells, cultured in LB with ampicillin. Upon induction with IPTG, the cultures were incubated with shaking overnight at 30 °C, followed by pelleting by centrifugation. The pellets were resuspended in buffer (300 × 10⁻³ M NaCl, 50 × 10⁻³ M Tris, pH 8) containing protease inhibitors (Complete, EDTA-free, Roche) and lysed through repeated flash freeze/defrost cycles, followed by fine probe-tip sonication of 2 × 5 min with 0.5 s on/off cycles at 0 °C, using Sartorius stedim biotech Labsonic P sonicator. Fine sonicator tip was essential to minimise protein loss through sample overheating and mechanical stress. Cell debris were subsequently removed by 45 min × 10000 g centrifugation at 4 °C. The proteins were isolated from the supernatant using Strep-Tactin affinity resin following the manufacturer's guidelines and subsequently purified by size exclusion chromatography on ÄKTApure purifier with GE Fraction collector F9-R, using HiLoad 16/600 Superdex 75 pg column and eluting with 300 × 10⁻³ M NaCl, 30 × 10⁻³ M Tris buffer, pH 8.

LmrR-S Binding Determination and Stability Measurements: UV-vis absorption spectra were recorded using Jasco V-630Bio spectrometer. Binding was monitored by absorbance of the S maximum peak shift in the presence of each LmrR mutant at room temperature in a 1 cm pathlength quartz cuvette. Stock solution of 600 × 10⁻⁶ M of S in acetonitrile was prepared. From the stock solution 5 × 10⁻⁶ M of S in

50 × 10⁻³ M NaCl, 50 × 10⁻³ M phosphate buffer, pH 8 was prepared with 1% of acetonitrile as co-solvent. The 5 × 10⁻⁶ M S solution was titrated with each protein mutant to achieve LmrR:S ratio of 0.2–4. The absorbance shift or absorbance decay as the LmrR:S ratio varied was monitored and fitted to saturation growth model (Equation (1)). The apparent dissociation constants for electrostatic and hydrophobic interaction (i.e., K_{de} and K_{dh}) were obtained from the fitting

$$\Delta A = \frac{\Delta \lambda_{\max} X}{X + K_d} \quad (1)$$

where $\Delta \lambda_{\max}$ is the maximum spectral change, X is LmrR:S ratio, and K_d is the dissociation constant.

UV-vis absorption over time was recorded using a Varioscan Flash plate reader from ThermoScientific. In a 96 well plate, 9 samples of 7.5 × 10⁻⁶ M S in 50 × 10⁻³ M NaCl, 50 × 10⁻³ M phosphate buffer, pH 8, (1% MeCN) and 9 samples for each LmrR protein mutant of 7.5 × 10⁻⁶ M S in the presence of 30 × 10⁻⁶ M LmrR were prepared (4:1 LmrR:S ratio). Absorbance measurements were monitored over time from 1 day to 1 month.

LmrR-S Complex Formation: A saturated solution of S in acetonitrile was prepared (≈600 × 10⁻⁶ M). LmrR in 100 × 10⁻³ M NaCl, 5 × 10⁻³ M EDTA, 20 × 10⁻³ M Tris buffer, pH 8, was placed in a dialysis bag and dialyzed against buffer of the same composition. Every 20 min, an aliquot of S solution, equal to 1% of the dialysis bag volume, was added to the LmrR solution, allowing acetonitrile to dissipate. Addition was repeated until precipitation of S was visible in the dialysis bag. The LmrR solution was then centrifuged for 10 min at 3000 g to remove the precipitate and the LmrR-S complex in the supernatant was concentrated using Amicon Ultra-4 (YM-3000) centrifugal filter devices from Millipore, purified using PD-10 size exclusion columns eluting with, 100 × 10⁻³ M NaCl, 1 × 10⁻³ M EDTA, 20 × 10⁻³ M Tris buffer, pH 8, and concentrated again.

Protein Crystallization: Crystallization was carried out using hanging-drop vapor-diffusion method using EasyXtal 15-Well plates from Qiagen. LmrR-S (15 mg mL⁻¹) in 100 × 10⁻³ M NaCl, 1 × 10⁻³ M EDTA, 20 × 10⁻³ M Tris buffer, pH 8, was mixed in 2:1 or 1:1 ratio with reservoir solution. The concentration of LmrR-S was based on protein content prior to complex formation, assuming no losses. The reservoir solution contained 12% PEG 3350, 5 × 10⁻³ M MgCl₂, 5 × 10⁻³ M CdCl₂, 5 × 10⁻³ M NiCl₂, 100 × 10⁻³ M Hepes, pH 7.5. Crystals suitable for crystallography were obtained within a week. Crystals were cryoprotected in reservoir solution containing 20% glycerol v/v. Diffraction data were collected at BL13-XALOC beamline at ALBA synchrotron as a contiguous sequence of 0.1° rotations using 1.48459 Å wavelength (Ni absorption edge). Structure refinements were carried out on *refmac* 5.8.0257 as implemented in CCP4. Model was built with *Coot*, initial phases were obtained with *phaser* using a published structure, PDB ID: 3f8b, as an initial model. Nickel ion positions were determined from anomalous scattering data. Coordinates of S for refinement were constructed using PRODRG server.^[57]

Characterization Techniques: UV circular dichroism (CD) spectra were recorded using a JASCO J-815 CD spectrometer with the protein in 50 × 10⁻³ M phosphate buffer at pH 8 in a 1 cm path length quartz cuvette, with and without S. A band-width of 1 and 1 nm increment were used in all cases. The photophysical characterization (emission spectra, η) was carried out with a FS5 Spectrofluorometer from Edinburgh Instruments, with SC-5 module for liquid samples, SC-10 module for solid samples, and SC-30 Integrating Sphere to determine ϕ ($\lambda_{exc} = 590$ nm). All measurements were performed at room temperature.

Theoretical Methods: The W96-S protein model was built using as starting structure the LmrR crystallographic structure obtained as described in *Protein crystallisation*. A protein monomer was built from the dimeric X-ray crystallographic structure using the C and D chains. Missing amino acids in chains C and D were added when the equivalent ones were available in the structure as well as a conformer of S. This model was used to build the W96A-S mutant

by replacing the tryptophan 96 by alanine in both chains. Both LmrR-S systems were subsequently completed inserting hydrogens and Na⁺ atoms to ensure electroneutrality and placed in a truncated octahedral solvent box of water with at least a 10 Å buffer of water molecules around the systems. All these transformations were carried out using Coot,^[58] UCSF Chimera^[59] and the AMBER 20 suite of programs.^[60]

Molecular Dynamics Simulations: QM/MM/MD simulations were performed using the electrostatic embedding approach as implemented in the AMBER 20 simulation suite.^[60] In detail, molecular mechanics methods were used to model the protein (Amber ff14SB force field^[61]), the water molecules (tip3p force field^[62]), and sodium cations (Joung/Cheatham ion parameters set^[63]), while the density-functional tight-binding method DFTB2^[64,65] was used to describe S. The remaining parameters needed for the van der Waals term in the QM/MM coupling Hamiltonian were taken from the general amber force field (gaff).^[66] Equilibration of the system started by relaxing the water molecules, the Na⁺ and S and imposing weak harmonic constraints on the protein residues using a combination of steepest descent and conjugate gradient methods. After this initial minimization step, the harmonic constraints were removed and the whole system was allowed to relax. In total, 25000 minimization steps were carried out. After that, 30 ps dynamics in the NVT ensemble were used to heat the system up to 300 K with an integration time of 0.5 fs and weak harmonic constraints applied to the protein. Next, 10 ns of equilibration in the NPT at 1 atm and 300 K using the Langevin thermostat and the Berendsen barostat^[67] and an integration time of 2 fs. After that, a production run of 40 ns was carried out using the same conditions as those employed in the last step of the equilibration process.

Device Preparation and Characterization: All reagents were purchased from Sigma-Aldrich, specifically: 1,1,1-Tris-(hydroxymethyl)-propanethoxylat (TMPE; M_n : ≈450) and polyethylene oxide (PEO; M_n : ≈5 × 10⁶). The rubber-like coatings were prepared with a mass ratio 4:1 (TMPE:PEO). A solution of S (10⁻³ mg mL⁻¹) and W96-S (10 mg mL⁻¹) was added to TMPE and stirred together with PEO to reach the same amount of emitters. The sample was dried overnight in a vacuum chamber at 3 mbar. The devices were fabricated using 590 nm LED chips (Future Eden) as pumping source. To carry out the photostability and conversion measurements the biophosphors were placed either on chip or remote (2 cm from the LED chip) configuration and driving at either different currents to study conversion and temperature or at 50 mA for long-term stability at ambient conditions. The electro-luminescence spectra were recorded through Avantes Spectrometer 2048L (300 VA grating, 200 μm slit, CCD detector) coupled with an AvaSphere 30-Irrad Integrated sphere, monitoring the temperature using a thermographic camera FLIR ETS320. The employed power source was a Keithley 2231-A-30-3.

Supporting Information

Supporting Information is available from the Wiley Online Library or from the authors.

Acknowledgements

S.F., S.H.M. and M.L. contributed equally to this work. The authors acknowledge the European Union's Horizon 2020 research and innovation FET-OPEN under grant agreement ARTIBLED No. 863170. R.D.C. acknowledges the ERC-Co InOutBioLight No. 816856. P.B.C. acknowledges financial support from the Ministry of Science, Innovation and Universities of Spain under the Beatriz Galindo Programme (No. MCIU-19-BEAGAL 18/0224), from MCIN/AEI/10.13039/501100011033 grant No. PGC2018-095953-B-I00 and from the Technical University of Munich (TUM) under the TUM Global Visiting Professor Programme. A.L.C. acknowledges support by the European Research Council ERC-CoG-648071-ProNANO and ERC-PoC-841063-NIMM; and Agencia Estatal

de Investigación, Spain (No. PID2019-111649RB-I00). This work was performed under the Maria de Maeztu Units of Excellence Program from the Spanish State Research Agency Grant No. MDM-2017-0720 (CIC biomAGUNE). Protein crystals were grown at the Macromolecular Crystallography Platform at CIC bioGUNE with the support of Dr. Adriana Rojas. X-ray diffraction experiments were performed at XALOC beamline at ALBA Synchrotron with the collaboration of ALBA staff. C.B. and G.R. acknowledge support by Progetti di Ricerca di Ateneo Ex-Post Anno 2018.

Open access funding enabled and organized by Projekt DEAL.

Correction added on 1 February 2022, after first online publication: the affiliation "Technische Universität München" was added for Aitziber Cortajarena.

Conflict of Interest

The authors declare no conflict of interest.

Data Availability Statement

The data that support the findings of this study are available in the supplementary material of this article.

Keywords

artificial fluorescent proteins, biohybrid light-emitting diodes, color down-conversion, deep-red biophosphors, protein-based lighting

Received: November 9, 2021

Revised: December 21, 2021

Published online: January 17, 2022

- [1] D. H. Flores, J. M. Anderson, *LEDs and Solid-State Lighting: Energy Savings Potential and a Manufacturing Roadmap*, Nova Science Publishers, Inc., New York 2012.
- [2] M. Hansen, K. Lee, V. Nubbe, M. Pattinson, Lighting R&D Program: LED Materials and Devices R&D Meeting, 2020.
- [3] M. Pattinson, M. Hansen, N. Bardsley, C. Elliott, K. Lee, L. Pattison, J. Tsao, 2019 Lighting R&D Opportunities, 2020.
- [4] M. Bidikoudi, E. Fresta, R. D. Costa, *Chem. Commun.* 2018, 54, 8150.
- [5] L. Wang, R.-J. Xie, T. Suehiro, T. Takeda, N. Hirotsuki, *Chem. Rev.* 2018, 118, 1951.
- [6] Y.-C. Lin, M. Karlsson, M. Bettinelli, *Top. Curr. Chem.* 2016, 374, 21.
- [7] G. Hong, X. Gan, C. Leonhardt, Z. Zhang, J. Seibert, J. M. Busch, S. Bräse, *Adv. Mater.* 2021, 33, 2005630.
- [8] S. S. Swayamprabha, D. K. Dubey, Shahnawaz, R. A. K. Y., M. R. Nagar, A. Sharma, F.-C. Tung, J.-H. Jou, *Adv. Sci.* 2021, 8, 2002254.
- [9] E. Fresta, V. Fernández-Luna, P. B. Coto, R. D. Costa, *Adv. Funct. Mater.* 2018, 28, 1707011.
- [10] Y. Zhang, J. Mei, C. Yan, T. Liao, J. Bell, Z. Sun, *Adv. Mater.* 2020, 32, 1902806.
- [11] H. Zhang, H. Zhang, A. Pan, B. Yang, L. He, Y. Wu, *Adv. Mater. Technol.* 2021, 6, 2000648.
- [12] D. Kong, K. Zhang, J. Tian, L. Yin, X. Sheng, *Adv. Mater. Technol.* 2021, 2100006.
- [13] W. Li, Q. Liu, Y. Zhang, C. Li, Z. He, W. C. H. Choy, P. J. Low, P. Sonar, A. K. K. Kyaw, *Adv. Mater.* 2020, 32, 2001591.

- [14] V. Fernández-Luna, P. B. Coto, R. D. Costa, *Angew. Chem., Int. Ed.* **2018**, *57*, 8826.
- [15] E. Gu, H. X. Zhang, H. D. Sun, M. D. Dawson, A. R. Mackintosh, A. J. C. Kuehne, R. A. Pethrick, C. Belton, D. D. C. Bradley, *Appl. Phys. Lett.* **2007**, *90*, 2005.
- [16] G. Heliotis, G. Itskos, R. Murray, M. D. Dawson, I. M. Watson, D. D. C. Bradley, *Adv. Mater.* **2006**, *18*, 334.
- [17] O. Kim, S. Ha, J. Il Kim, J. Lee, *ACS Nano* **2010**, *4*, 3397.
- [18] I. O. Huyal, U. Koldemir, T. Ozel, H. V. Demir, D. Tuncel, *J. Mater. Chem.* **2008**, *18*, 3568.
- [19] F. Hide, P. Kozodoy, S. P. DenBaars, A. J. Heeger, *Appl. Phys. Lett.* **1997**, *70*, 2664.
- [20] J. Lee, V. C. Sundar, J. R. Heine, M. G. Bawendi, K. F. Jensen, *Adv. Mater.* **2000**, *12*, 1102.
- [21] H. F. Xiang, S. C. Yu, C. M. Che, P. T. Lai, *Appl. Phys. Lett.* **2003**, *83*, 1518.
- [22] Y. Cui, T. Song, J. Yu, Y. Yang, Z. Wang, G. Qian, *Adv. Funct. Mater.* **2015**, *25*, 4796.
- [23] L. Niklaus, H. Dakhil, M. Kostrzewa, P. B. Coto, U. Sonnewald, A. Wierschem, R. D. Costa, *Mater. Horiz.* **2016**, *3*, 340.
- [24] C. Ezquerro, E. Fresta, E. Serrano, E. Lalinde, J. García-Martínez, J. R. Berenguer, R. D. Costa, *Mater. Horiz.* **2019**, *6*, 130.
- [25] A. A. Wiles, J. Bruckbauer, N. Mohammed, M. Cariello, J. Cameron, N. J. Findlay, E. Taylor-Shaw, D. J. Wallis, R. W. Martin, P. J. Skabara, G. Cooke, *Mater. Chem. Front.* **2020**, *4*, 1006.
- [26] Y. Duan, C. Ezquerro, E. Serrano, E. Lalinde, J. García-Martínez, J. R. Berenguer, R. D. Costa, *Adv. Funct. Mater.* **2020**, *30*, 2005401.
- [27] J. Chen, J. Wang, X. Xu, J. Li, J. Song, S. Lan, S. Liu, B. Cai, B. Han, J. T. Precht, D. Ginger, H. Zeng, *Nat. Photonics* **2020**, *15*, 238.
- [28] M. D. Weber, L. Niklaus, M. Pröschel, P. B. Coto, U. Sonnewald, R. D. Costa, *Adv. Mater.* **2015**, *27*, 5493.
- [29] A. Espasa, M. Lang, C. F. Aguiño, D. Sanchez-deAlcazar, J. P. Fernández-Blázquez, U. Sonnewald, A. L. Cortajarena, P. B. Coto, R. D. Costa, *Nat. Commun.* **2020**, *11*, 879.
- [30] M. S. P. Reddy, C. Park, *Sci. Rep.* **2016**, *6*, 32306.
- [31] K. Benson, A. Ghimire, A. Pattammattel, C. V. Kumar, *Adv. Funct. Mater.* **2017**, *27*, 1702955.
- [32] D. Zhou, H. Zou, M. Liu, K. Zhang, Y. Sheng, J. Cui, H. Zhang, B. Yang, *ACS Appl. Mater. Interfaces* **2015**, *7*, 15830.
- [33] H. Tetsuka, A. Nagoya, R. Asahi, *J. Mater. Chem. C* **2015**, *3*, 3536.
- [34] L. Niklaus, S. Tansaz, H. Dakhil, K. T. Weber, M. Pröschel, M. Lang, M. Kostrzewa, P. B. Coto, R. Detsch, U. Sonnewald, A. Wierschem, A. R. Boccaccini, R. D. Costa, *Adv. Funct. Mater.* **2017**, *27*, 1601792.
- [35] V. Fernández-Luna, D. Sánchez-de Alcazar, J. P. Fernández-Blázquez, A. L. Cortajarena, P. B. Coto, R. D. Costa, *Adv. Funct. Mater.* **2019**, *29*, 1904356.
- [36] X. Wang, Y. Guo, Z. Li, W. Ying, D. Chen, Z. Deng, X. Peng, *RSC Adv.* **2019**, *9*, 9777.
- [37] X. Wang, Z. Li, W. Ying, D. Chen, P. Li, Z. Deng, X. Peng, *J. Mater. Chem. C* **2019**, *8*, 240.
- [38] A. Aires, V. Fernández-Luna, J. Fernandez-Cestau, R. D. Costa, A. L. Cortajarena, *Nano Lett.* **2020**, *20*, 2710.
- [39] D. Sanchez-deAlcazar, D. Romera, J. Castro-Smirnov, A. Sousaraei, S. Casado, A. Espasa, M. C. Morant-Miñana, J. J. Hernandez, I. Rodríguez, R. D. Costa, J. Cabanillas-Gonzalez, R. V. Martinez, A. L. Cortajarena, *Nanoscale Adv.* **2019**, *1*, 3980.
- [40] V. Fernández-Luna, J. P. Fernández-Blázquez, M. A. Monclús, F. J. Rojo, R. Daza, D. Sanchez-Dealcazar, A. L. Cortajarena, R. D. Costa, *Mater. Horiz.* **2020**, *7*, 1790.
- [41] T. J. Lambert, *Nat. Methods* **2019**, *16*, 277.
- [42] R. N. Day, M. W. Davidson, *Chem. Soc. Rev.* **2009**, *38*, 2887.
- [43] U. K. Sukumar, A. Natarajan, T. F. Massoud, R. Paulmurugan, *Top. Med. Chem.* **2019**, *34*, 149.
- [44] S. H. Mejías, G. Roelfes, W. R. Browne, *Phys. Chem. Chem. Phys.* **2020**, *22*, 12228.
- [45] S. V. C. Butnarusu, N. Barbero, C. Barolo, *Dyes Pigm.* **2021**, *184*, 108873.
- [46] N. Barbero, C. Magistris, J. Park, D. Saccone, P. Quagliotto, R. Buscaino, C. Medana, C. Barolo, G. Viscardi, *Org. Lett.* **2015**, *17*, 3306.
- [47] Y. Xu, Z. Li, A. Malkovskiy, S. Sun, Y. Pang, *J. Phys. Chem. B* **2010**, *114*, 8574.
- [48] G. M. Paternò, L. Moretti, A. J. Barker, C. D'Andrea, A. Luzio, N. Barbero, S. Galliano, C. Barolo, G. Lanzani, F. Scotognella, *J. Mater. Chem. C* **2017**, *5*, 7732.
- [49] J. Park, C. Barolo, F. Sauvage, N. Barbero, C. Benzi, P. Quagliotto, S. Coluccia, D. Di Censo, M. Grätzel, M. K. Nazeeruddin, G. Viscardi, *Chem. Commun.* **2012**, *48*, 2782.
- [50] C. Gude, W. Rettig, *J. Phys. Chem. A* **2000**, *104*, 8050.
- [51] G. M. Paternò, N. Barbero, S. Galliano, C. Barolo, G. Lanzani, F. Scotognella, R. Borrelli, *J. Mater. Chem. C* **2018**, *6*, 2778.
- [52] L. Villarino, K. E. Splan, E. Reddem, L. Alonso-Cotchico, C. Gutiérrez de Souza, A. Lledós, J.-D. Maréchal, A.-M. W. H. Thunnissen, G. Roelfes, *Angew. Chem., Int. Ed.* **2018**, *57*, 7785.
- [53] C. Mayer, C. Dulson, E. Reddem, A.-M. W. H. Thunnissen, G. Roelfes, *Angew. Chem., Int. Ed.* **2019**, *58*, 2083.
- [54] P. K. Madoori, H. Agustindari, A. J. M. Driessen, A.-M. W. H. Thunnissen, *EMBO J.* **2009**, *28*, 156.
- [55] J. P. van der Berg, P. K. Madoori, A. G. Komarudin, A.-M. Thunnissen, A. J. M. Driessen, *PLoS One* **2015**, *10*, e0135467.
- [56] C. F. Aguino, M. Lang, V. Fernández-Luna, M. Pröschel, U. Sonnewald, P. B. Coto, R. D. Costa, *ACS Omega* **2018**, *3*, 15829.
- [57] A. W. Schüttelkopf, D. M. F. Van Aalten, *Acta Cryst. D* **2004**, *60*, 1355.
- [58] P. Emsley, K. Cowtan, *Acta Cryst. D* **2004**, *60*, 2126.
- [59] E. F. Pettersen, T. D. Goddard, C. C. Huang, G. S. Couch, D. M. Greenblatt, E. C. Meng, T. E. Ferrin, *J. Comput. Chem.* **2004**, *25*, 1605.
- [60] D. A. Case, H. M. Aktulga, K. Belfon, I. Y. Ben-Shalom, S. R. Brozell, D. S. Cerutti, T. E. Cheatham III, G. A. Cisneros, V. W. D. Cruzeiro, T. A. Darden, R. E. Duke, G. Giambasu, M. K. Gilson, H. Gohlke, A. W. Götz, R. Harris, S. Izadi, S. A. Izmailov, C. Jin, K. Kasavajhala, M. C. Kaymak, E. King, A. Kovalenko, T. Kurtzman, T. S. Lee, S. LeGrand, P. Li, C. Lin, J. Liu, T. Luchko, et al., *Amber 2021*, University of California, San Francisco **2021**.
- [61] J. A. Maier, C. Martinez, K. Kasavajhala, L. Wickstrom, K. E. Hauser, C. Simmerling, *J. Chem. Theory Comput.* **2015**, *11*, 3696.
- [62] W. L. Jorgensen, J. Chandrasekhar, J. D. Madura, R. W. Impey, M. L. Klein, *J. Chem. Phys.* **1998**, *79*, 926.
- [63] I. S. Joungh, T. E. Cheatham, III, *J. Phys. Chem. B* **2008**, *112*, 9020.
- [64] M. Elstner, D. Porezag, G. Jungnickel, J. Elsner, M. Haugk, T. Frauenheim, S. Suhai, G. Seifert, *Phys. Rev. B* **1998**, *58*, 7260.
- [65] M. Elstner, G. Seifert, *Phil. Trans. R. Soc. A* **2014**, *372*, 20120483.
- [66] J. Wang, R. M. Wolf, J. W. Caldwell, P. A. Kollman, D. A. Case, *J. Comput. Chem.* **2004**, *25*, 1157.
- [67] H. J. C. Berendsen, J. P. M. Postma, W. F. van Gunsteren, A. DiNola, J. R. Haak, *J. Chem. Phys.* **1998**, *81*, 3684.